Available online at www.sciencedirect.com
ScienceDirect
Polymer 48 (2007) 6719–6727
polymer
www.elsevier.com/locate/polymer

Gas transport in ethylene–propylene–diene (EPDM) elastomer: Molecular simulation and experimental study

S.W. Rutherford*, D.T. Limmer, M.G. Smith, K.G. Honnell

Los Alamos National Laboratory, Los Alamos, NM 87545, USA

Received 14 February 2007; received in revised form 3 July 2007; accepted 5 July 2007
Available online 15 July 2007

Abstract

Time lag permeation measurements with ethylene–propylene–diene (EPDM) elastomer have been undertaken in an effort to characterize the gas transport properties of this barrier material. The derived solubility and diffusivity of a series of probe gases including helium, hydrogen, neon, argon, krypton, oxygen, nitrogen, carbon dioxide and methane were measured and compared with molecular simulation predictions. Molecular Dynamics (MD) and Grand Canonical Monte Carlo (GCMC) calculations were performed to provide estimates for diffusivity and solubility, respectively. Agreement between the molecular simulations and experimental data is obtained for simple spherical monatomic probe gases, with greater deviation observed for non-spherical polyatomic gases. Additionally, agreement between semi-empirical correlations based on the effective cross-sectional area of the diffusing species and the effective Lennard–Jones interaction constant of the sorbed species is better than widely used correlations based on gas critical properties. Furthermore, the molecular simulations provide a meaningful representation for the elastomer studied and additionally appear to capture the fundamental principles of sorption and diffusion of the chosen probe gases.
Published by Elsevier Ltd.

Keywords: Solubility; Diffusivity; Permeability

1. Introduction

Ethylene–propylene–diene (EPDM) elastomer has become a barrier material of significant commercial importance due to its superior resistance to thermal, oxidative and radiation degradation coupled with its ability to accommodate high volume fractions of filler and liquid plasticizers [1]. Although this elastomer is primarily used in the automotive, electrical and industrial construction industries, new applications in commercial separation and purification industries [2–6] are also being forged. Increasing demand has resulted in a market for this elastomer that accounted for 12% of the world's consumption of synthetic rubber in 2002 [7]. As of 2003, EPDM was the world's fastest growing general purpose elastomer [7] and growth is expected to continue beyond 2006 [8].

Despite its importance in sealing and separation applications, a fundamental understanding of transport through EPDM is still incomplete. Further investigation is required to obtain accurate, fully predictive models that are capable of estimating the solubility and diffusivity of gases in this elastomer. Construction of a successful model can result in the prediction of selectivity in membrane separation operations and aid progress in the quantification of aging rates when diffusion limited oxidation is observed [9,10]. To this end, molecular simulations have provided a useful tool in developing fundamental structure–property relationships that can yield fully predictive models.

Significant progress has been made over the last 20 years in the exploration, by molecular simulation, of polymers as membrane materials for separation operations [11]. Based on a given chemical architecture, a novel synthetic polymer can theoretically be developed and scrutinized for its utility as a separation medium. This concept offers enormous potential for development in the material sciences. This fact, coupled

* Corresponding author. Tel.: +1 505 6640812; fax: +1 505 6640815.
E-mail address: stevenr@lanl.gov (S.W. Rutherford).

0032-3861/$ - see front matter Published by Elsevier Ltd.
doi:10.1016/j.polymer.2007.07.020

with increasing computational power and efficiency, allows macromolecular design to be brought to a wider range of users. However, there are still some challenges that must be overcome in the use of molecular simulation as a tool for membrane design [12]. Accurate and robust forcefield development is a major challenge that is currently being addressed. An existing forcefield, known as COMPASS (condensed phase optimized molecular potentials for atomistic simulation studies) [13] has been explored in the prediction of gas diffusion and solubility in rubbery and glassy polymers [14–19]. The predictive accuracy of this forcefield has not been robustly established for a wide range of polymers and probe gases, and further validation work is therefore beneficial. Additionally, to the best of the authors' knowledge, no previous studies have been undertaken to explore the capability of molecular simulation prediction for gas solubility and diffusivity in EPDM. As a contribution to this end, grand canonical Monte Carlo (GCMC) and molecular dynamics (MD) simulations are undertaken in this investigation, in conjunction with the COMPASS forcefield, to provide estimates of diffusivity and solubility of four monatomic gases (He, Ne, Ar and Kr) and five polyatomic gases (H_2, N_2, CO_2, O_2 and CH_4) in EPDM terpolymer. The predicted values for solubility and diffusivity are compared with experimental values gathered by the time lag permeation method and used to assess the predictive capability of the techniques and associated forcefield. Furthermore, several previously proposed correlations for solubility and diffusivity are also assessed for their predictive capability.

2. Materials and methods

2.1. Experimental methodology

Ethylene–propylene–diene terpolymer containing 5-ethylidene norbornene (ENB) as the cross-linking diene was synthesized according to the procedure outlined in a previous publication [20]. EPDM has been previously studied for gas solubility using volumetric batch sorption uptake method. However, this method reaches limitations when probing low solubility gases, due to the fact that limited quantities of gas are sorbed at room temperature. An alternative method that can be employed for low solubility gases is the time lag permeation technique [21]. In this investigation, a time lag permeation apparatus was constructed and employed to characterize the diffusivity and solubility of He, Ne, Kr, N_2, H_2 and Ar. With the exception of argon, these gases have not been previously studied in EPDM terpolymer containing ENB. Argon permeation experiments were undertaken to provide comparison and validation with previously obtained batch uptake data for diffusivity and solubility.

The time lag permeation apparatus is designed for single species permeation and operates at pressures up to 1000 torr. Each component of the experimental apparatus is fitted with Swagelok VCR face seal fittings for minimum system leak. Leak testing of this system indicates a maximum leak rate that is multiple orders of magnitude below the lowest permeation rate measured in this investigation. The gas flow in the system is regulated using Swagelok BG series valves capable of operating under high pressures and high vacuum. The pressure transducers are MKS Baratron type 615A high accuracy sensor head with a maximum pressure of 10 torr on the downstream and 1000 torr on the upstream and an accuracy of 0.12% of reading. The pressure signal is fed through an MKS high accuracy signal conditioner of type 270D and logged to a computer using National Instruments hardware and Labview software with a logging frequency of one point per second. The system vacuum is maintained by a Varian turbo pump (V70LP) backed by a Varian mechanical diaphragm pump (MDP-30). The manufacturer rates the ultimate pressure of this vacuum ensemble at less than 10^{-9} torr.

The time lag permeation method requires monitoring the downstream pressure rise while the upstream is kept effectively constant [21]. Additionally, the magnitude of the downstream pressure is kept much less than the upstream pressure in order for an effective steady state of flow to result. In this investigation, the downstream pressure never exceeds 0.1% of the upstream pressure and the experiment is run for a period of at least 10 times the observed time lag. All experiments are conducted at a temperature of 293 K. A minimum of three replicate permeation experiments for each gas are undertaken in order to obtain mean and standard deviation values.

The ethylene–propylene–diene terpolymer used in the study has a 53:47 ethylene to propylene ratio with 5-ethylidene norbornene (ENB) included as the diene. Curing agents and antioxidants are added to the polymer in the form of Dicup 40C (Dicumyl peroxide), SR-350 (Trimethylolpropane trimethacrylate), Zic-Stick '85' (Zinc oxide) and Flectol (polymerized 1,2-dihydro-2,2,4-trimethylquinoline). According to Noordermeer [22], EPDM with roughly equal ethylene to propylene ratio should yield a level of crystallinity at room temperature of less than 1%, possess a glass transition temperature below −50 °C and should therefore be predominantly amorphous. The EPDM employed in this study has been characterized by X-ray diffraction [23] and is consistent with this hypothesis.

The sample thickness was measured using a low measuring force Sylvac Z_CAL 150 Height Gauge (supported by a Granite plate) whose resolution is stated at 0.0005 inches (1 μm) and accuracy 0.0015 inches (4 μm). The mean thickness is 0.067 cm with a standard deviation of 4%. The elastomer, which has a density of 0.97 ± 0.04 g/cc, was initially outgassed for 15 days at room temperature by exposing to pressures below the measurable range of the pressure transducers (i.e. $<10^{-5}$ torr). Between permeation experiments, the samples were outgassed for at least 24 h.

Gases were supplied by Valley Gas & Specialty Equipment (Ultra-pure H_2 at 99.999% purity, Ultra-pure N_2 at 99.999% purity, Ultra-pure Ar at 99.999% purity) and Air Liquide (Research grade Kr at 99.998% purity, Research grade Ne at 99.999% purity, Research grade He at 99.999% purity).

2.2. Molecular simulation methodology

2.2.1. COMPASS forcefield

The COMPASS forcefield describes potential energy of a system as a function of atomistic configuration while allowing for bond stretching, bond angle bending, bond rotation, and for non-bonded interactions such as van der Waals and Coulombic interactions [13]. This proprietary forcefield was originally developed from the polymer consistent force field (PCFF) by re-parametrization of the non-bond parameters. The COMPASS forcefield has been applied to model phosphazenes [24] and to estimate solubility in polyolefins [25]. It has also been employed to predict solubility and diffusivity in poly(2,6-dimethyl-1,4-phenylene oxide) [14] in poly(organophosphazenes) [17,18] and in polyacetylenes [15,16]. For further details regarding the COMPASS forcefield, the reader is directed to a publication by Sun [13].

2.2.2. Simulation of polymer structure

In this investigation, MD simulations are initially performed in order to obtain a representative relaxed EPDM structure. MD simulations utilizing the NVT ensemble are engaged for this purpose and are performed with Materials Studio 4.0 software, produced by Accelrys Inc. Initially, a polymer chain was produced using the "Build Polymer" function of Materials Studio. A random copolymer was built using the random copolymer option. This option is based on the stipulation of probability for monomer insertion into the polymer chain. Small differences in composition for each build can result due to the random nature of the build. This is intended to mimic a random reaction of ethylene, propylene and diene units. The occurrence probability for each unit was specified in accordance with the formulation details.

The chain was constructed with 50 repeat units, which consisted of ethylene, propylene and ENB. In light of a study by Takeuchi [26] which showed only a small difference between oxygen diffusion in a volume of infinite chain length and diffusion in a volume containing a chain of 20 segments, a 50 repeat unit structure was assumed to be sufficient to obtain representative behavior. Eight uncrosslinked chains were then packed into a cubic volume of length between 2.3 and 2.7 nm (depending on cell target density chosen) using the amorphous cell module at the target density using a self-avoiding walk algorithm [27]. The presence of cross-links is not directly considered in the molecular simulations. However, cross-linking is expected to affect solute transport primarily through its effect on the packing of polymer chains and therefore the resulting polymer density. The molecular simulations capture the measured density of the crosslinked polymer, thereby indirectly incorporating an important result of the presence of cross-links.

The unit cell is effectively surrounded on all sides by replicas of itself to minimize finite size effects. This unit cell can then be employed in GCMC simulations to determine gas solubility, or alternatively, employed in further MD simulations to examine gas diffusivity.

2.2.3. MD simulations for diffusion coefficients

In MD simulations aimed at the determination of self-diffusivity, four of the chosen probe molecules were randomly added to the unit cell. This was followed by minimization of the potential energy of the penetrant/polymer system. All interactions between the atoms of the polymer chains, between polymer chains and diffusing penetrant molecules, and between the penetrant molecules themselves are taken into account. This was accomplished by means of the Discover software employing the COMPASS forcefield. In the present study, the potential energy function for the non-bonded interactions was truncated at an interatomic distance of 12.5 Å. Additionally, these non-bond interactions were computed using a charge group based summation method [28]. These groups were made up of forcefield assigned charge groups. At this stage, the total energy of the generated polymer structure is minimized using "smart minimizing method" [28] run for 20 000 steps. The resulting structure is then equilibrated by NVT-MD simulations at 293 K in order to ensure that its minimized total energy remains approximately constant with respect to the simulation time.

Diffusion coefficients of He, H_2, Ne, Ar, Kr, O_2, N_2, CO_2, and CH_4 in the equilibrated EPDM structure were determined from MD simulations. These simulations are performed within the framework of the NVE ensemble. A time step of 1 fs has been used in the NVE–MD simulations. Mean-square displacements (MSDs) of He, H_2, Ne, Ar, Kr, O_2, N_2, CO_2 and CH_4 were calculated from the trajectories of four penetrant molecules of the same species in EPDM with output every 200 fs. The self-diffusivity, which is equivalent to the measured Fickian diffusivity at infinite dilution [29], is then determined from the diffusion relation [30]:

$$D = \lim_{t\to\infty} \frac{\left\langle |\vec{r}(t) - \vec{r}(0)|^2 \right\rangle}{6t} = \lim_{t\to\infty} \left\{ \frac{\mathrm{MSD}}{6t} \right\} \tag{1}$$

In this investigation the MSD data was analyzed up to 1000 ps (1 ns). However, anomalous diffusion is observed in the first 200 ps. This period is then followed by diffusive motion that obeys Eq. (1) at times greater than 200 ps. This is shown in Fig. 1, where the MSD initially increases rapidly at short times, followed by a period that follows the diffusion relation defined by Eq. (1).

The NVE–MD simulations for self-diffusivity are chosen over NVT–MD simulations which can artificially alter the dynamics by introducing non-physical effects [31]. In fact, computation in the NVE ensemble is recommended by Dubbeldam et al. [31] for single particle diffusion coefficients unless a large number of particles are used. A disadvantage of the NVE–MD calculation is the temperature drift which occurred from the starting temperature of 293 K. The drift was consistently increasing during the first 200 ps which was observed to be the anomalous diffusion regime. The magnitude of the rise varied for each gas but was between 4 and 6 K. After 200 ps, outside the anomalous diffusion regime, the temperature drift was much less and was no greater than 1 K for the remaining simulation period, for all gases. The final simulation temperature

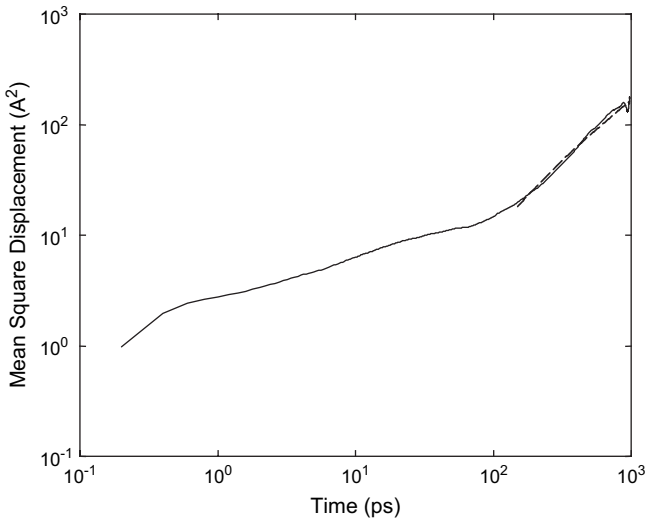

Fig. 1. Mean-square displacement for neon atoms in EPDM, showing the conformance, after 200 ps, to the diffusion limit represented as the dashed line.

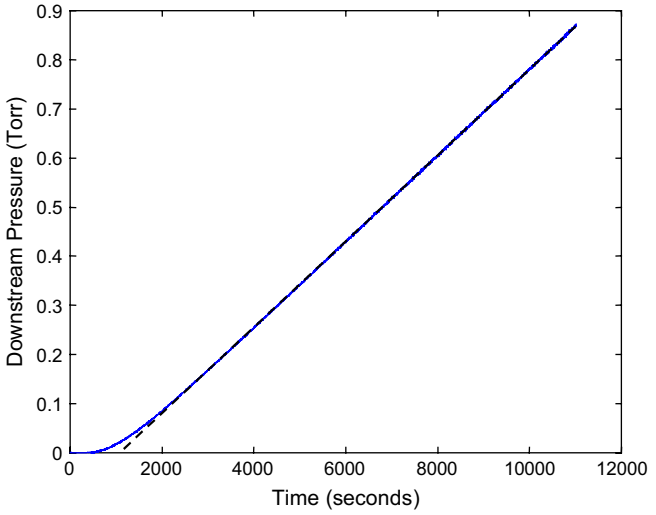

Fig. 2. Downstream pressure rise for argon permeation through EPDM indicating that the experiment is continued for at least 10 times the observed time lag. The dashed line represents the steady state asymptote and its intercept with the abscissa yields the diffusivity.

therefore varied and the diffusivity values reported in this investigation are quoted between 297 and 299 K.

2.2.4. GCMC simulation for sorption isotherm

After constructing the polymer system (Section 2.2.2), the configurational energy is minimized using ''smart minimizing method'' [28] followed by equilibration using NVT–MD. The equilibrated cell was subsequently used for GCMC simulations employing the standard Metropolis algorithm [32,33] using the ''Sorption Isotherm'' module [28]. All GCMC simulations were conducted at a temperature of 293 K and employed 10^7 steps. The GCMC calculations of this investigation are similar to those performed by Fried and Ren [17], Hu and Fried [18], Holck et al. [34], Heuchel et al. [35] and Liu and Huang [36] who have also employed the COMPASS forcefield. These simulations treat the sorbate and polymer as rigid, with only rigid body translations and reorientations allowed. The GCMC calculation is therefore carried out over a single configurational ''snapshot'' of the polymer system.

3. Results and discussion

3.1. Diffusivity

The time lag permeation apparatus allows simultaneous determination of permeability (P_e) and diffusivity (D) in the EPDM elastomer. A typical downstream pressure rise from the time lag permeation experiment is indicated for argon in Fig. 2. The pressure rise approaches the steady state asymptote indicated as a straight line whose slope yields the permeability. The intercept of the steady state asymptote with the abscissa is known as the time lag (t_{lag}) from which the diffusivity is calculated as [37]:

$$D = \frac{L^2}{6t_{lag}} \tag{2}$$

where L is the polymer thickness. These experiments are conducted for a series of simple monatomic gases (He, Ne, Ar, and Kr) together with non-spherical probe gases (H_2 and N_2). Additionally, these data can be combined with results from a prior study that presents data for O_2, CO_2, Ar and CH_4 on the same material [20]. The measured diffusivity is presented in Table 1 and compared with the simulation results of Section 2.2.3. The standard deviation for diffusivity (ς_D) is calculated as a function of the standard deviation in thickness (ς_L) and standard deviation in the time lag measurement ($\varsigma_{t_{lag}}$) as:

$$\left(\frac{\varsigma_D}{D}\right)^2 = \left(\frac{2\varsigma_L}{L}\right)^2 + \left(\frac{\varsigma_{t_{lag}}}{t_{lag}}\right)^2 \tag{3}$$

The experimental value for argon obtained in this study agrees, within error, with the value obtained in a prior investigation ($5.0 + -1.4 \times 10^{-7}$ cm^2/s) [20] using the batch uptake method.

3.1.1. Diffusivity of monatomic gases in EPDM

The diffusion of solute molecules in simple liquids has been well described by the Stokes–Einstein relation popularized by Wilke and Chang [38]. A variety of studies furthering the work of Wilke and Chang [38] have shown that the diffusion on non-swelling probe gases in polymers can also be correlated through the Stokes–Einstein relation [39–43]. These studies seek to relate diffusivity, at a fixed temperature, to the critical volume of the probe gas. Despite the many theoretical limitations imposed by this relationship, this correlation appears to have worked reasonably well in application to gas diffusion in polymers. The relationship is expressed as:

$$D = \frac{\lambda}{V_c^{\eta}} \tag{4}$$

Table 1
Summary of simulated and experimentally derived values

Gas	T_c (K)	V_c (cc/mol)	$(\varepsilon/k)_{eff}$ (K)	σ_{TM} (nm)	P_e [b] (ccSTP cm/cm^2 s cmHg)	D_{sim} (cm^2/s)	D_{exp} [b] (cm^2/s)	S_{sim} (ccSTP/cc atm)	S_{exp} [b] (ccSTP/cc atm)
He	5.21	57.8	9.50	0.178	2.8×10^{-9} (10%)	1.7×10^{-5}	1.7×10^{-5} (11%)	8.7×10^{-3}	1.3×10^{-2} (15%)
H_2	33.2	65.1	62.2	0.214	4.2×10^{-9} (10%)	3.3×10^{-5}	8.0×10^{-6} (10%)	3.2×10^{-2}	4.0×10^{-2} (14%)
Ne	44.5	41.8	27.1	0.23	8.0×10^{-9} (8%)	4.1×10^{-6}	4.9×10^{-6} (11%)	2.1×10^{-2}	1.8×10^{-2} (14%)
Ar	151.2	74.6	122.3	0.297	1.0×10^{-9} (6%)	6.6×10^{-7}	6.4×10^{-7} (11%)	2.1×10^{-2}	1.2×10^{-1} (13%)
N_2	126.2	90.1	83.0	0.304	5.0×10^{-10} (6%)	2.3×10^{-7}	5.5×10^{-7} (10%)	2.7×10^{-3}	7.0×10^{-2} (12%)
Kr	209.0	92.3	176.6	0.322	2.1×10^{-9} (9%)	2.9×10^{-7}	3.4×10^{-7} (9%)	3.4×10^{-4}	4.6×10^{-1} (13%)
CO_2	304.2	93.1	213.4	0.302	5.3×10^{-9} [a]	6.5×10^{-7}	3.6×10^{-7}	2.8×10^{-1}	1.12 [a]
O_2	154.4	73.4	112.7	0.289	8.8×10^{-10} [a]	1.2×10^{-7}	6.5×10^{-7}	2.9×10^{-2}	1.04×10^{-1} [a]
CH_4	190.7	99.2	154.7	0.318	9.5×10^{-10} [a]	7.6×10^{-7}	2.3×10^{-7}	4.2×10^{-3}	3.14×10^{-1} [a]

[a] Taken from Ref. [20].
[b] Mean value with percent standard deviation included.

where V_c is the critical volume of the mobile species, and λ and η are adjustable parameters. For simple spherical probe molecules, this relationship is shown in Fig. 3. Eq. (4) predicts that the gas with the highest diffusivity should be neon, followed by helium, argon and krypton. However, the measured values for diffusivity indicate the following decreasing order for monatomic gases: helium, neon, argon and krypton. This correlation therefore fails to predict the correct order of diffusivity for simple monatomic gases.

Another popular correlation for diffusivity has been established by Teplyakov and Meares [44] and relates the diffusivity to the effective cross-sectional area of the solute. Table 1 contains the values of effective diameter supplied by Teplyakov and Meares [44], denoted σ_{TM}. Fig. 4 shows the correlation of diffusivity with the molecular cross-sectional area represented by the square of this diameter. It is evident that the data for monatomic gases is well characterized by this correlation which can predict the correct order for diffusivity.

Also appearing on Fig. 4 is the calculated diffusivity value obtained from MD simulation. The simulated values not only agree with the Teplyakov–Meares correlation but are also in near quantitative agreement with the experimental values. In general, predictive accuracy of MD simulations has been quoted with two to three orders of magnitude discrepancy between experimental and predicted values [45]. In the early 1990s, one to two orders of magnitude were considered to be the standard, due to inaccuracies in the early use of united-atom forcefields [12]. More recently, an order of magnitude accuracy was quoted for diffusion in PEI [46] and a ''factor of three to five'' was quoted as acceptable accuracy [47]. In this respect, the accuracy of the predictions in this study for monatomic gases in EPDM is noteworthy. Moreover, the previously mentioned semi-empirical correlations employ adjustable parameters which must be calibrated to produce an accurate correlation. The prediction of diffusivity obtained from MD simulations, for a given forcefield, does not require calibration against the diffusion data and is therefore considered to be fully predictive. Considering the accuracy of this fully predictive molecular model, it appears that MD simulations based on the COMPASS forcefield, effectively capture the essential nature of monatomic solute transport in EPDM.

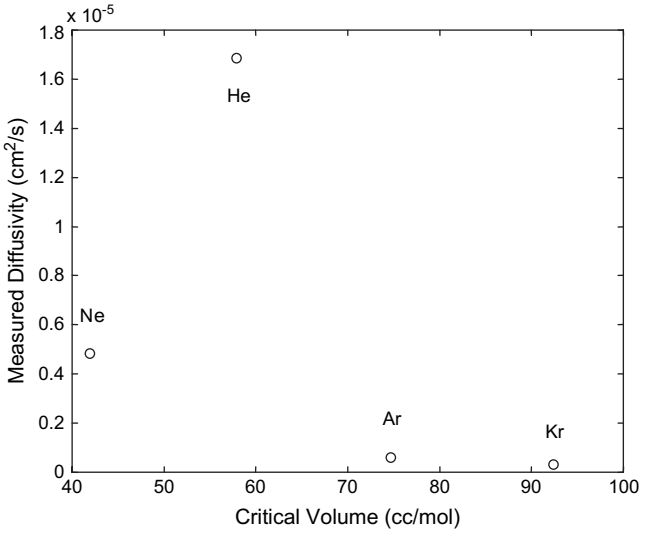

Fig. 3. Measured values for diffusivity of monatomic gases in EPDM plotted against critical volume.

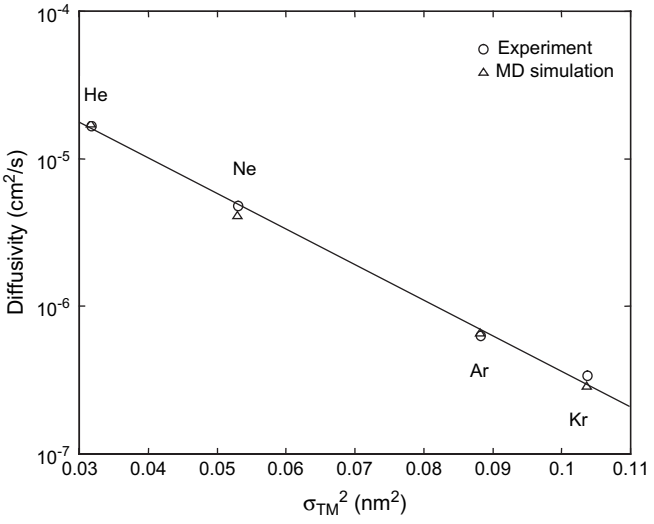

Fig. 4. Mean values for diffusivity of monatomic gases in EPDM together with the value predicted by molecular dynamics plotted against the square of the diameter. The solid line represents the fit to experimental data for monatomics.

3.1.2. Diffusivity of polyatomic gases in EPDM

The diffusion of simple monatomic probe gases appear to conform to the correlation proposed by Teplyakov and Meares [44] and is quantitatively predicted by MD simulations. However, for non-spherical polyatomic probes where consideration of penetrant shape is important, the correlation and MD simulations are found to be less accurate, as shown in Fig. 5.

In many diffusion correlations, including the Stokes–Einstein relation, effective diameters are assigned to non-spherical probes. The effective size can be inferred through the application of a variety of potential models, such as Lennard–Jones potential. An effective diameter can therefore depend on the potential model employed and the nature of the van der Waals interactions. For example, a 'kinetic diameter', calculated from the minimum cross-sectional area, can be employed as a measure of molecular size [48]. These values can vary significantly from the values of effective diameter quoted by Teplyakov and Meares [44]. Considering the non-uniqueness and variability in effective size introduced by non-spherical probes, the correlation maintains a reasonable predictive capability.

The results of molecular dynamics calculations also shown in Fig. 5 indicate a similar difficulty with polyatomic gases. The lack of accuracy in estimates for diffusivity has been previously attributed to the process of potential parameter fitting [46]. It has been proposed that the parameters of PCFF forcefield, the precursor of COMPASS, have been optimized to describe polymer morphology at the expense of accuracy in transport property prediction [46]. This may explain the lack of predictive accuracy. Despite this, these calculations are still within the 'factor of three to five' accuracy typically observed in MD simulations.

3.2. Solubility

Gas solubility (S) is determined from the measured permeability and diffusivity through the assumption that the solution-diffusion [49] mechanism is obeyed:

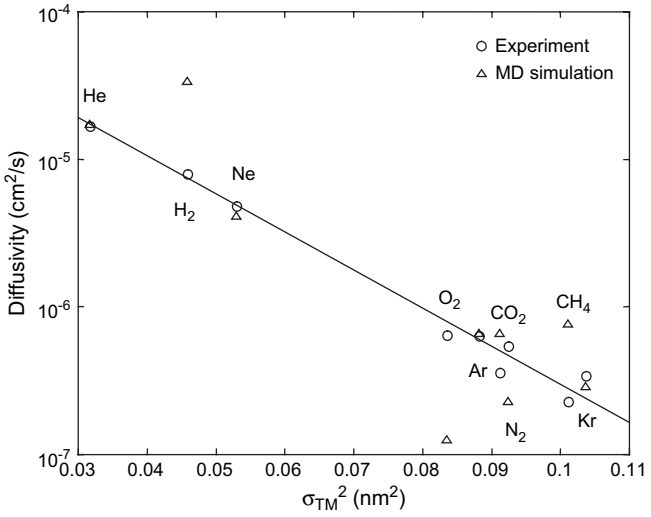

Fig. 5. Mean values for diffusivity in EPDM together with the value predicted by molecular dynamics plotted against the square of the diameter. The solid line represents the fit to experimental data for all gases.

$$S = \frac{P_e}{D} \tag{5}$$

The mean values for permeability and solubility appear in Table 1. The estimates for standard deviation, also appearing in Table 1, are determined by considering that the most significant source of error in the calculated permeability (P_e) is variability in measured steady state pressure rise ($\dot{p}$), in upstream pressure (p_o) (which has a variation no greater than 2%) and in thickness (which has a standard deviation estimated at 4%). Other sources of uncertainty are error in downstream volume and membrane cross-sectional which are estimated at less than 1% and are therefore not considered. The standard deviation for permeability ς_{P_e}, is then calculated as:

$$\left(\frac{\varsigma_{P_e}}{P_e}\right)^2 \approx \left(\frac{\varsigma_{\dot{p}}}{\dot{p}}\right)^2 + \left(\frac{\varsigma_{p_0}}{p_o}\right)^2 + \left(\frac{\varsigma_L}{L}\right)^2 \tag{6}$$

and the standard deviation for solubility ς_S, is calculated as:

$$\left(\frac{\varsigma_S}{S}\right)^2 = \left(\frac{\varsigma_{P_e}}{P_e}\right)^2 + \left(\frac{\varsigma_D}{D}\right)^2 \tag{7}$$

In a previous study, argon solubility in this material was quoted at 0.11 ± 0.01 ccSTP/cc/atm [20], in agreement with the results obtained in this investigation at the same temperature.

Prediction of gas solubility within rubbery polymers has commonly been undertaken using critical temperature of the probe gas as a measure of molecular interaction [50]. van Amerongen [50] has extensively explored this relationship through assessment of solubility data on a variety of gases and rubbers. From a theoretical standpoint, the critical temperatures of the probe gases studied can be considered to be a measure of van der Waals interaction between molecules. A larger critical temperature corresponds to larger van der Waals interaction [51]. On this basis, van Amerongen [50] has fitted the solubility for a range of gases, with the best-fit result given by:

$$\ln S = 0.017 T_c - 4.7 \tag{8}$$

where solubility (S) is in units of ccSTP/cc/atm and critical temperature (T_c) is in Kelvin. This empirical correlation has some success in describing the solubility for a series of gases in a variety of glassy and rubbery polymers [50,52]. A theoretical basis for this correlation has been examined by some authors [53] and appears to be theoretically plausible for monatomic gases. Eq. (8) predicts a linear relationship between the natural logarithm of the solubility and the critical temperature of the probe gas. This plot is shown in Fig. 6 and the best fit of the data analyzed in this investigation yields:

$$\ln S = 0.015 T_c - 4.2 \tag{9}$$

This result is close to van Amerongen's [50] correlation, however, there is some considerable deviation from the line of best fit. Additionally, this correlation predicts the following order

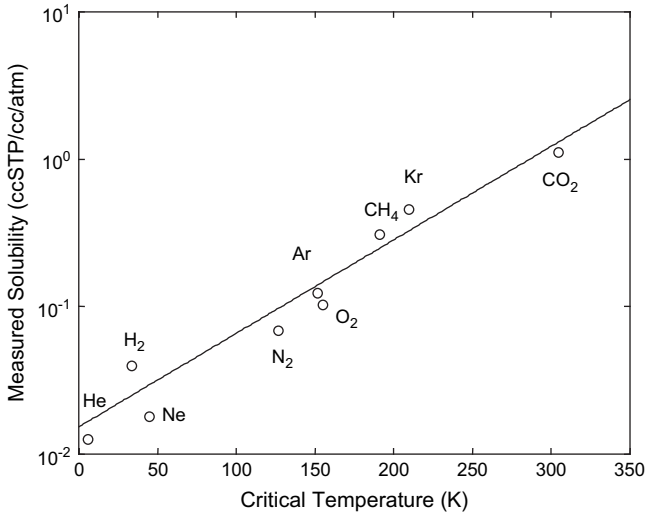

Fig. 6. Correlation of measured solubility with critical temperature of the probe gas.

for gas solubility from least soluble to most soluble: $He < H_2 < Ne < N_2 < Ar < O_2 < CH_4 < Kr < CO_2$. In contrast, the measured order of gas solubility is $He < Ne < H_2 < N_2 < O_2 < Ar < CH_4 < Kr < CO_2$.

Another well studied correlation for solubility has been provided by Teplyakov and Meares [44] and relates an effective Lennard–Jones interaction constant, $(\varepsilon/k)_{\text{eff}}$, to solubility through:

$$\ln S = K_1 + K_2\left(\frac{\varepsilon}{k}\right)_{\text{eff}} \tag{10}$$

where K_1 and K_2 are fitting parameters. Fig. 7 indicates that this correlation performs reasonably well with significantly less deviation than the critical temperature correlation.

Additionally, it succeeds in predicting the correct order of the solubility. The reason for the superior performance could be partially ascribed to the method by which the effective Lennard–Jones interaction constants are obtained. Teplyakov and Meares [44] have provided mean values for these parameters based on fitting of data for more than 50 polymeric materials [54,55]. The effectiveness of this correlation is likely to be enhanced by the semi-empirical nature of the data fitting procedure that is employed.

Estimated values for solubility in EPDM can also be provided by GCMC simulations employing the COMPASS forcefield. These simulations yield sorption isotherms shown in Fig. 8. In all cases the isotherms appear to be linear within the fugacity range shown, indicating equilibrium conforming to Henry's law. The slopes of the isotherms are used to calculate the solubilities and Table 1 contains the calculated solubilities obtained by GCMC simulation. The values obtained from these simulations are plotted in Fig. 9. It is evident that these values for probe gases such as He, Ne and H_2 are in reasonable agreement with the experimental data. However, for probe gases of larger size, considerable deviation is observed. The GCMC simulations appear to be consistently under-predicting the solubility for the larger probe molecules. The largest deviation is observed for Kr, followed by CH_4, N_2, CO_2, Ar and O_2. Notably, this is also the order of decreasing molecular size. This fact, coupled with the consistent under prediction, indicates that limitations with the GCMC sampling procedure for larger molecules are being encountered. These limitations are manifested in the inability to accurately estimate solute chemical potential when the insertion of large test particles is attempted in free volume elements of size comparable with molecular size, a problem referred to as the "insertion problem" by Theodorou [30].

In order to further explore this effect we have generated EPDM matrices of varying densities less than the mean sample density including 0.9525, 0.935 and 0.9175 g/cc. Sorption isotherms are calculated in these simulated polymers and the results are shown in Fig. 10. This plot indicates that the solubility for the larger molecules consistently increases as density

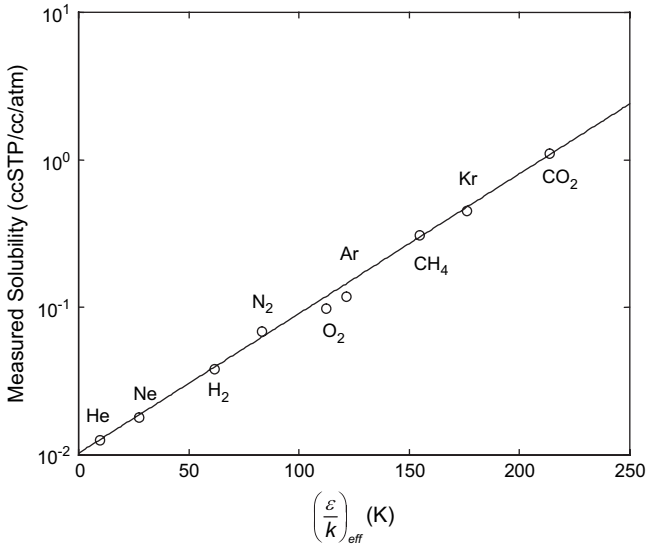

Fig. 7. Correlation of measured solubility against effective Lennard–Jones interaction constant.

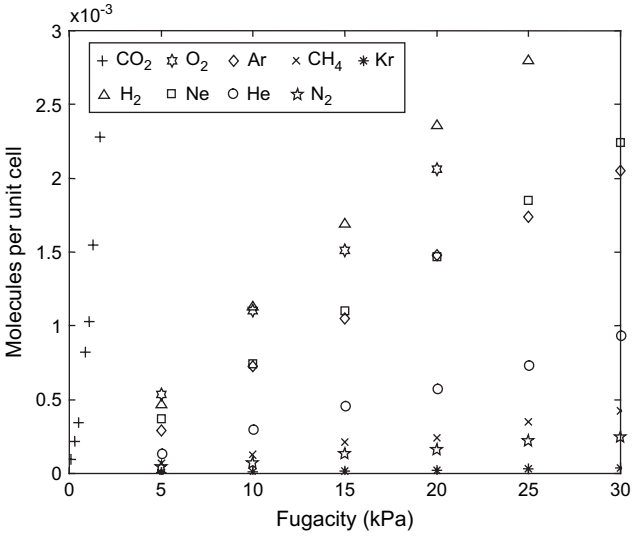

Fig. 8. Predicted sorption isotherms obtained from GCMC.

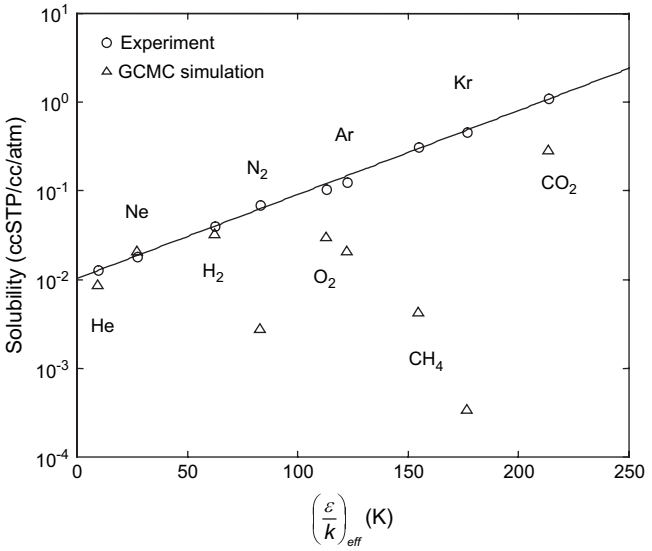

Fig. 9. Correlation of measured and predicted solubilities against effective Lennard–Jones interaction constant.

decreases. Also apparent from Fig. 10 is the fact that solubility increases as polymer density decreases. This result is consistent with free volume theories which predict that increases in fractional free volume lead to increase in solubility [11]. Fig. 10 also indicates that, at the lowest chosen density (0.9175 g/cc), the solubility increases with an increasing value of the effective Lennard–Jones interaction constant. At this density, the simulated result is consistent with the experimental data trend. This suggests that the simulated free volume elements are large enough to allow effective sampling with the large probe molecules in the GCMC algorithm. The ''insertion problem'' is apparently ameliorated at this density which is approximately 5% lower than the mean sample density.

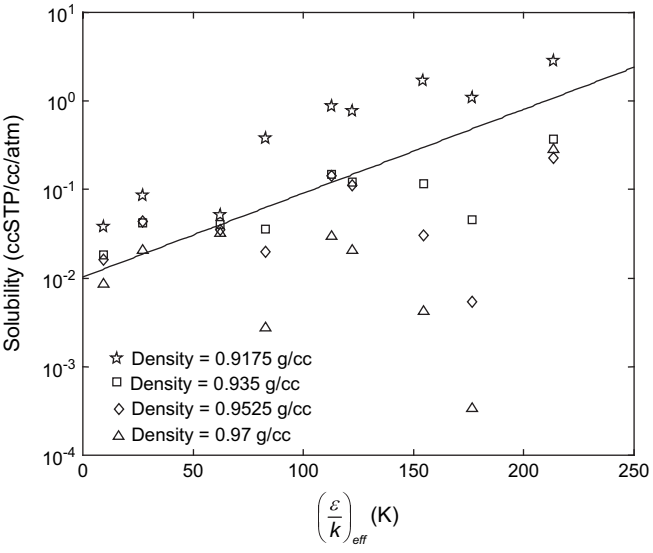

Fig. 10. Correlation of calculated solubility against effective Lennard–Jones interaction constant for simulated EPDM with varying density. Solid line represents the line of best fit to the experimental data.

Despite the intrusion of the 'insertion problem' for larger molecules, the GCMC simulations can successfully represent the solubility of smaller helium, neon and hydrogen and are within an order of magnitude for nitrogen, oxygen, argon and carbon dioxide.

4. Conclusions

Through assessment of helium, neon, argon and krypton, the diffusivity of simple, spherical, monatomic species in EPDM are well correlated with molecular cross-sectional area. In contrast, the critical volume of the monatomic species provides a correlation for diffusivity that cannot account for the order in which diffusivity is predicted to increase. MD simulations for diffusivity of the monatomics in EPDM are in near quantitative agreement with experimental data obtained in this investigation. Diffusivities of polyatomic species including hydrogen, nitrogen, oxygen and methane are less capably represented by effective cross-sectional areas when compared with predictions for monatomics. Molecular dynamics predictions for diffusivity of polyatomic species deviate further from experimental data than predictions for monatomics but are still within a reasonable margin.

The solubility of all probe gases is well correlated by an effective Lennard–Jones interaction constant, which provides a more capable representation of data than the commonly employed critical temperature correlation. For small solute molecules, GCMC calculations for solubility are in reasonable agreement with experimental data. For larger molecules, the ''insertion problem'' is observed and appears to be overcome at densities approximately 5% lower than the measured value of the EPDM sample studied.

Based on the prediction of solubility and diffusivity, molecular simulations employing the COMPASS forcefield provide a reasonable representation of EPDM terpolymer and capture the essential elements of solute interaction for the range of gases studied.

References

[1] Encyclopedia of polymer science and engineering, vol. 6. New York: John Wiley & Sons; 1986.
[2] Pereira CC, Habert AC, Nobrega R, Borges CP. J Membr Sci 1998;138:227–35.
[3] Meuleman EEB, Willemsen JHA, Mulder MHV, Strathmann H. J Membr Sci 2001;188:235–49.
[4] Meuleman EEB, Bosch B, Mulder MHV, Strathmann H. AIChE J 1999; 45:2153.
[5] Netke SA, Sawant SB, Joshi JB, Pangarkar VG. J Membr Sci 1994;91: 163.
[6] Huang RYM, Moon GY, Pal R. Ind Eng Chem Res 2002;41:531.
[7] Burridge E. Eur Chem News 2003;82:16.
[8] Tullo AH. Chem Eng News 2005;83:21–4.
[9] Gillen KT, Clough RL. Polymer 1992;33:4358.
[10] Celina M, Gillen KT. Macromolecules 2005;38:2754.
[11] Stern SA. J Membr Sci 1994;94:1.
[12] Muller-Plathe F. Acta Polym 1994;45:259–93.
[13] Sun H. J Phys Chem B 1998;102:7338–64.
[14] Fried JR, Sadat-Akhavi M, Mark JE. J Membr Sci 1998;149:115–26.

[15] Wang XY, Raharjo RD, Lee HJ, Lu Y, Freeman BD, Sanchez IC. J Phys Chem 2006;110:12666–72.
[16] Kucukpinar E, Doruker P. Polymer 2003;44:3607–20.
[17] Fried JR, Ren P. Comput Theor Polym Sci 2000;10:447–63.
[18] Hu N, Fried JR. Polymer 2005;46:4330–43.
[19] Zhou JH, Zhu RX, Zhou JM, Chen MB. Polymer 2006;47:5206–12.
[20] Rutherford SW, Kurtz RE, Smith MG, Honnell KG, Coons JE. J Membr Sci 2005;63:57–65.
[21] Rutherford SW, Do DD. Adsorption 1997;3:283–312.
[22] Noordermeer JWM. Ethylene–propylene polymers, Encyclopedia of polymer science and technology. John Wiley & Sons; 2002. p. 1–17.
[23] Orler EB, Williams DJ, Wrobleski DA, Smith MG, unpublished work.
[24] Sun H, Ren P, Fried JR. Compt Theor Polym Sci 1998;8:229.
[25] Kanellopoulos V, Mouratides D, Pladis P, Kiparissides C. Ind Eng Chem Res 2006;45:5870.
[26] Takeuchi H. J Chem Phys 1990;93:4490–1.
[27] Theodorou DN, Suter UW. Macromolecules 1985;18:1467.
[28] Introduction to polymer modeling: training manual, Version April 2006. San Diego: Accelrys Software Inc.; 2006.
[29] Churati C, Stern SA. Macromolecules 1998;31:5529–35.
[30] Theodorou DN. In: Yampolski Y, Pinnau I, Freeman BD, editors. Principles of molecular simulation of gas transport in polymers in material science of membranes. John Wiley and Sons; 2006.
[31] Dubbeldam D, Beerdsen E, Vlugt TJH, Smit B. J Chem Phys 2005; 122:224712.
[32] Metropolis N, Rosenbluth AW, Rosenbluth MN, Teller AH, Teller E. J Chem Phys 1953;21:1087.
[33] Allen MP, Tildesley DJ. Computer simulation of liquids. New York: Oxford; 1987. p. 118–23, 126–31.
[34] Holck O, Siegert MR, Heuchel M, Bohning M. Macromolecules 2006; 39:9590–604.
[35] Heuchel M, Bohning M, Holck O, Siegert MR, Hofmann D. J Polym Sci Part B Polym Phys 2006;44:1874.
[36] Liu QL, Huang Y. J Phys Chem B 2006;110:17375.
[37] Crank J. The mathematics of diffusion, vol. 1. Oxford, UK: Oxford University Press; 1975.
[38] Wilke CR, Chang P. AIChE J 1955;1:264.
[39] Lin HQ, Freeman BD. Macromolecules 2006;39:3568–80.
[40] Lin HQ, Kai T, Freeman BD, Kalakkunnath S, Kalika DS. Macromolecules 2005;38:8381.
[41] Prabhakar RS, De Angelis MG, Sarti GC, Freeman BD, Coughlin MC. Macromolecules 2005;38:7043.
[42] Prabhakar RS, Freeman BD, Roman I. Macromolecules 2004;37: 7688.
[43] Serad GE, Freeman BD, Stewart ME, Hill AJ. Polymer 2001;42:6929.
[44] Teplyakov V, Meares P. Gas Sep Purif 1990;4:66–74.
[45] Muller-Plathe F, Rogers SC, van Gunsteren WF. Macromolecules 1992;35:6722.
[46] Lim SY, Tsotsis TT, Sahimi M. J Chem Phys 2003;119:496.
[47] Hofmann D, Fritz L, Ulbrich J, Schepers C, Bohning M. Macromol Theory Simul 2000;9:293.
[48] Breck DW. Zeolite molecular sieves. New York: Wiley; 1974.
[49] Wigmans JG, Baker RW. J Membr Sci 1995;107:1–21.
[50] van Amerongen GJ. Rubber Chem Technol 1964;37:1067.
[51] McQuarrie DA. Statistical mechanics. New York: Harper & Row; 1973. p. 243–45.
[52] Merkel TC, Bondar VI, Nagai K, Freeman BD, Pinnau I. J Polym Sci Part B Polym Phys 2000;38:413.
[53] Curro JG, Honnell KG, McCoy JD. Macromolecules 1997;30:145.
[54] Teplayakov VV, Durgayan SG. Vskomolek Soed 1985;27A:818.
[55] Volkov VV, Nametkin NS, Novitsky EG, Durgayan SG. Vskomolek Soed 1979;21A:920.